



Published in final edited form as:

Mol Cell. 2010 July 9; 39(1): 145–151. doi:10.1016/j.molcel.2010.06.027.

Structure of the endonuclease domain of MutL: unlicensed to cut

Monica C. Pillon¹, Jessica J. Lorenowicz¹, Michael Uckelmann², Andrew D. Klocko³, Ryan R. Mitchell¹, Yu Seon Chung¹, Paul Modrich^{4,5}, Graham C. Walker⁶, Lyle A. Simmons³, Peter Friedhoff², and Alba Guarné^{1,*}

¹ Department of Biochemistry and Biomedical Sciences, McMaster University, Hamilton, Ontario L8N 3Z5, Canada

² Institut für Biochemie (FB 08), Justus-Liebig-Universität, D-35392 Giessen, Germany

³ Department of Molecular, Cellular, and Developmental Biology, University of Michigan, Ann Arbor MI 48103

⁴ Department of Biochemistry, Duke University Medical Center, Durham NC 27710

⁵ Howard Hughes Medical Institute, Duke University Medical Center, Durham NC 27710

⁶ Department of Biology, Massachusetts Institute of Technology, Cambridge MA 02139

Summary

DNA mismatch repair corrects errors that have escaped polymerase proofreading, increasing replication fidelity 100- to 1000-fold in organisms ranging from bacteria to humans. The MutL protein plays a central role in mismatch repair by coordinating multiple protein-protein interactions that signal strand removal upon mismatch recognition by MutS. Here we report the crystal structure of the endonuclease domain of *Bacillus subtilis* MutL. The structure is organized in dimerization and regulatory subdomains connected by a helical lever spanning the conserved endonuclease motif. Additional conserved motifs cluster around the lever and define a Zn²⁺-binding site that is critical for MutL function *in vivo*. The structure unveils a powerful inhibitory mechanism to prevent undesired DNA nicking and allows us to propose a model describing how the interaction with MutS and the processivity clamp could license the endonuclease activity of MutL. The structure also provides a molecular framework to propose and test additional roles of MutL in mismatch repair.

* Correspondence to: Alba Guarné, Department of Biochemistry and Biomedical Sciences, HSC-4N57A, McMaster University, 1200 Main Street West, Hamilton, ON L8N 3Z5, Canada., Phone: 1 (905) 525-9140 (x26394), FAX: 1 (905) 522-9033, guarnea@mcmaster.ca.

Accession Numbers

Atomic coordinates and structure factors of BsMutL-CTD have been deposited in the Protein Data Bank (accession code 3GAB, 3KDG, 3KDK).

Supplemental Information

Supplemental Data include Supplemental Experimental Procedures, three figures, one movie and one table that can be found with this article online.

Publisher's Disclaimer: This is a PDF file of an unedited manuscript that has been accepted for publication. As a service to our customers we are providing this early version of the manuscript. The manuscript will undergo copyediting, typesetting, and review of the resulting proof before it is published in its final citable form. Please note that during the production process errors may be discovered which could affect the content, and all legal disclaimers that apply to the journal pertain.

Keywords

DNA mismatch repair; MutL; endonuclease; HNPCC; β -clamp

Introduction

DNA mismatch repair (MMR) maintains genomic stability by correcting errors that have escaped polymerase proofreading (Kunkel and Erie, 2005). MMR proteins are also implicated in a variety of other cellular processes such as DNA damage signaling, apoptosis, meiotic and mitotic recombination, and somatic hypermutation (Modrich, 2006). Mutations in mismatch repair genes are associated with an increased mutation rate and microsatellite instability, the hallmark of human non-polyposis colorectal cancer (Peltonmaki, 2005).

Initiation of MMR depends on the coordinated action of three proteins. MutS recognizes a mismatched base pair or a small insertion/deletion loop and recruits MutL in an ATP-dependent manner. Subsequently, the newly synthesized strand is marked for repair. In *Escherichia coli*, strand discrimination is achieved by mismatch-provoked activation of the MutH endonuclease, which cleaves the unmethylated DNA strand at hemimethylated GATC sites transiently generated during DNA replication. Although most bacteria and all eukaryotes do not encode a MutH homolog, a pre-existing nick is sufficient to activate mismatch repair in a system reconstituted from purified proteins (Zhang et al., 2005). It has been shown that MutL homologs from species lacking a MutH endonuclease harbor an intrinsic latent nicking endonuclease activity that is vital for its function in mismatch repair (Erdeniz et al., 2007; Kadyrov et al., 2006; Kadyrov et al., 2007; Kosinski et al., 2008).

MutL is composed of two structurally conserved domains connected by a variable flexible linker (Guarné et al., 2004). The N-terminal region encompasses an ATPase domain of the GH1 ATPase superfamily that is conserved from bacteria to humans (Ban et al., 1999; Guarné et al., 2001). Conversely, the sequence conservation in the C-terminal dimerization region of MutL is low. The structure of the C-terminal domain of *E. coli* MutL reveals that this region is organized into two distinct subdomains (Guarné et al., 2004; Kosinski et al., 2005).

While prokaryotic MutL homologs form homodimers, their eukaryotic counterparts form heterodimers. In humans, there are four paralogs of MutL (hMLH1, hPMS2, hPMS1 and hMLH3) that form three heterodimers by association of hMLH1 with hPMS2 (hMutL α), hPMS1 (hMutL β) and hMLH3 (hMutL γ) (Li and Modrich, 1995; Lipkin et al., 2000; Raschle et al., 1999). hMutL α is necessary for mismatch repair function and hMutL γ has a role in meiotic recombination, however the function of hMutL β is unknown (Kunkel and Erie, 2005). The C-terminal regions of hPMS2 and hMLH3 encompass a conserved DQHA(X)₂E(X)₄E motif that is required for endonuclease activity. Based on sequence analysis and molecular modelling, three additional conserved motifs (ACR, C(P/N)HGRP and FXR) have been predicted to form a single active site with the endonuclease motif (Kosinski et al., 2008). Analysis of the reconstituted human MMR system indicates that the endonuclease activity of MutL α provides a loading site for MutS α -activated exonuclease I (Kadyrov et al., 2006).

Here we present the structure of the C-terminal dimerization domain of *Bacillus subtilis* MutL (BsMutL) harboring the endonuclease activity of the protein. The structure reveals the conserved three-dimensional organization of the endonuclease site of MutL and exposes the presence of a regulatory Zn²⁺-binding site that is important for the mismatch repair function of BsMutL *in vivo*. The structure allows for us to propose a model describing how the

association of MutS and the DNA polymerase III processivity clamp (β -clamp), with MutL could license nicking of a newly synthesized DNA strand.

Results and Discussion

Crystal Structure of BsMutL-CTD

Three crystal forms of the C-terminal domain of BsMutL (BsMutL-CTD) were obtained. Crystal form I was used to determine the structure of BsMutL-CTD by multiwavelength anomalous diffraction using crystals grown with Sel-Met substituted protein (Table I). This crystal includes four independent monomers (molecules A to D) in the asymmetric unit that associate through crystal symmetry to form the functional BsMutL-CTD dimer. Crystal forms II and III contained a single dimer in the asymmetric unit. In the three structures, the N- and C-terminal ends of BsMutL-CTD (residues 433-461/580-627) define the dimerization subdomain, while residues 474-573 define an external subdomain that protrudes to the solvent, herein referred to as the regulatory subdomain (Figure 1A-B). The subdomains are connected by helix α A (residues 463-473), encompassing the conserved endonuclease motif, and the linker connecting helices α D- α E (residues 575-581), which is disordered in our structures (Figure 1A). However, the relative orientation between subdomains varies from one crystal form to another (Movie S1).

The three complementary conserved motifs associate with the endonuclease motif cluster around helix α A to delineate a single catalytic site with the conserved endonuclease motif (⁴⁶²DQHA(X)₂E(X)₄E) (Figure 1B-C). ⁶⁰⁴CPHGRP resides in the α E- β 8 loop, ⁵⁷²SCK (consensus sequence ACR) is the last turn of the α D helix and ⁶²³FKR, at the C-terminus of the protein, reaches the active site of the other protomer (Figure 1B). Except for the ⁵⁷²SCK motif, contributed by the regulatory subdomain, all motifs reside in the dimerization subdomain.

Two additional conserved motifs have been identified within the C-terminal region of MutL α (Kosinski et al., 2008). The ⁴⁴³GQ motif resides on the β 1 strand of the dimerization subdomain. This strand is in the vicinity of the α D- α E loop and hence it may indirectly contribute to the overall stability of the active site. The ⁴⁸⁷QEMIVP motif (consensus sequence QXLLXP) is on the surface of the regulatory subdomain and conspicuously exposed to the solvent (Figure 1B). Conservation of the QXLLXP motif is not correlated with the endonuclease activity of MutL, suggesting that it could mediate the interaction with other repair factors.

Even though the C-terminal regions of EcMutL and BsMutL have very low sequence similarity, their structures have nearly identical topologies (Figure S1). However, key differences exist. Superimposition of the EcMutL-CTD monomer onto the BsMutL-CTD monomer returned root mean squared deviations of only 1 Å for the dimerization subdomains but > 2 Å for the regulatory subdomains, reflecting the increased divergence of this region. This is intriguing because the regulatory subdomain contributes minimally to the endonuclease site. The most striking difference between the two structures is the organization of the secondary structure elements surrounding helix α A, which would preclude the formation of a functional endonuclease site even if EcMutL had the conserved DQHA(X)₂E(X)₄E motif (Figure S1). Notably, the extended α E- β 8 loop in BsMutL, rather than the additional helix seen in EcMutL, brings the ⁶⁰⁴CPHGRP motif closer to helix α A and secludes the endonuclease site. The dimerization interfaces are also remarkably different. While the BsMutL dimer buries 1,065 Å², the EcMutL dimer only conceals 910 Å². Interestingly, the reorientation of the apposing β -sheets in the BsMutL-CTD dimer allows the ⁶²³FKR motif to reach the adjacent endonuclease site.

BsMutL has weak endonuclease activity

Similarly to other MutL orthologues, BsMutL had a weak endonuclease activity dependent on Mn^{2+} (Figure 2A). Both a point mutation in the endonuclease motif (D462N) or deletion of the ATPase domain virtually abolished the endonuclease activity of BsMutL (Figure 2A). This finding is interesting in light of the recent experiments revealing that the C-terminal domains of *Neisseria gonorhoeae* and *Aquifex aeolicus* have endonuclease activity (Duppatla et al., 2009; Mauris and Evans, 2009). However, the specific activity of AaeMutL-CTD is much lower than that of the full-length protein. We suspected that the lack of nicking activity by BsMutL-CTD could be due to a DNA-binding defect, since EcMutL-CTD does not bind DNA stably (Guarné et al., 2004). Indeed, BsMutL-CTD did not bind supercoiled DNA while other variants of BsMutL did (Figure 2C).

Addition of 0.5 mM ATP stimulated the nicking activity of BsMutL, but higher concentrations of ATP (5 mM) inhibited the nicking activity, presumably due to excess nucleotide chelating Mn^{2+} ions away (Figure 2B, lanes 5 and 6). Unexpectedly, addition of ATP and/or Mg^{2+} stimulated a second cut on the nicked DNA to yield a linear product. The cut of the two strands at nearby points could be due to the presence of two endonuclease sites in the BsMutL homodimer or a consequence of the high-ion concentrations used in the experiment. We favor the former because incubation with 10 mM Mn^{2+} did not cause nicking of the two strands (data not shown), but addition of only 1 mM of a second metal ion such as Zn^{2+} or Co^{2+} yielded a linear product (Figure 2D). Interestingly, Mg^{2+} did not support double nicking under these conditions, suggesting that BsMutL may have higher affinity for Zn^{2+} or Co^{2+} than Mg^{2+} .

We then characterized the ATPase activity of BsMutL ($K_m = 0.4$ mM and $k_{cat} = 0.3$ min⁻¹) and found that it is a weaker ATPase than other MutL homologues (Ban et al., 1999; Guarné et al., 2001; Hall et al., 2002). Given the slow ATP-hydrolysis rate, the stimulation of the endonuclease activity of BsMutL was likely due to ATP-binding rather than ATP-hydrolysis. In good agreement with this idea, ADP did not stimulate the endonuclease activity of BsMutL (Figure 2B, lanes 9 and 10). However, two known non-hydrolyzable analogues of ATP, AMPPnP and ATP γ S, did not stimulate the endonuclease activity of BsMutL beyond the levels observed when both Mn^{2+} and Mg^{2+} were present either (Figure 2D, compare lanes 4, 7, 9 and 11). Conceivably, the ATP-dependent stimulation of the endonuclease activity of BsMutL could be due to a conformational change induced by ATP binding as seen in other MutL orthologues (Ban et al., 1999; Sacho et al., 2008), that would bring DNA bound at the ATPase domain in close proximity to the endonuclease site. If this is the case, our results suggest that only ATP can induce efficiently such conformational change.

BsMutL has a regulatory Zn^{2+} -binding site

Although the endonuclease activity of BsMutL was metal-dependent and the conserved motifs around helix αA define a putative Zn^{2+} -binding site (Kosinski et al., 2008), no metal ions were found in the BsMutL-CTD structure (crystal form I). However, different crystal forms were obtained when the protein storage buffer (crystal form II) and the crystallization solution (crystal form III) were supplemented with $ZnCl_2$. While the ⁴⁶²DQHA(X)₂E(X)₄E, ⁵⁷²SCK and ⁶⁰⁴C(P/N)HGRP motifs were much closer in crystal form II than crystal form I, no metal was found in this crystal form either. Conversely, the BsMutL-CTD dimer found in the asymmetric unit of crystal form III contained two Zn^{2+} ions bound to each protomer; a fully-occupied Zn^{2+} ion ($Zn^{2+}A$) was coordinated by the side chains of residues Glu468, Cys604, His606 and a well-ordered water molecule, and a partly occupied site ($Zn^{2+}B$) coordinated by the side chains of residues His464, Glu468, Cys573 and a water molecule (Figure 3A). The nature of the metal ion was confirmed on the

anomalous difference electron density maps from diffraction data collected at the Zn^{2+} absorption edge (Table I).

It had been previously reported that the putative Zn^{2+} -binding site in hPMS2 could be related to the regulatory metal-binding site found in the iron-dependent repressors from the DtxR/MntR family (Kosinski et al., 2008). A structural comparison revealed that, while motifs $^{462}DQHAX_2EX_4E$, ^{572}SCK and $^{604}CPHGRP$ from BsMutL could be superimposed to the regulatory metal-binding sites of IdeR or MntR, the residues coordinating the metal ion differed. However, another Mn^{2+} -dependent repressor from the same family (ScaR, PDB: 3HRU) encompasses a regulatory metal-binding site identical to the fully occupied Zn^{2+} site in BsMutL-CTD.

To probe whether the two metal-bound sites found in our structure were true Zn^{2+} -binding sites, we measured the affinity of purified BsMutL-CTD and various BsMutL-CTD variants for zinc. To this end, we measured the fluorescence of increasing concentrations of Zn^{2+} bound to the fluorescence indicator FluoZin-3. In the absence of protein, fluorescence increased exponentially reaching maximum values at around 1.5-2 μM $ZnCl_2$. The sigmoidal response observed for wild type and the D462N, H464S and E473K variants was characteristic of zinc binding by the protein (Figure 3B), suggesting that these BsMutL-CTD variants still retained the ability to bind zinc. Addition of the sulfhydryl-modifying agent methyl methanethiosulfonate (MMTS) resulted in an increase of fluorescence to the level detected in the absence of protein, indicating that one or more cysteine residues within the C-terminal domain of BsMutL were important for Zn^{2+} -binding (data not shown). Conversely, fluorescence profiles of E468K, C604A, H606S and C604A/H606S mutants did not have a sigmoidal response (Figure 3B), revealing that these BsMutL-CTD variants had lost the ability to bind zinc. These results confirmed that Glu468, Cys604 and His606 define the Zn^{2+} -binding site in BsMutL (Figure 3A).

Integrity of the conserved motifs is important for mismatch repair *in vivo*

We presumed that the integrity of the Zn^{2+} -binding site in MutL would be important for proper mismatch repair. Therefore, we measured the MMR efficiency of BsMutL variants encompassing point mutations in the conserved residues involved in the endonuclease or Zn^{2+} -binding sites. Mutation of D462A, H464A, E468K or H606A completely inactivated MMR *in vivo* (Figure 3C), underscoring the importance of these residues. Similarly, the equivalent mutations in hPMS2 also conferred a strong mutator phenotype (Kosinski et al., 2008). Conversely, the BsMutL-Q463A and BsMutL-E473K variants had similar mismatch repair efficiency to wild-type BsMutL, suggesting that not all the conserved residues within these motifs play essential roles in mismatch repair.

We next analyzed the importance of other conserved motifs found in the C-terminal region of MutL, namely the $^{487}QEMIVP$ motif. Mutation of Ile490 almost completely inactivated MMR *in vivo*, whereas mutation of Pro492 was without effect (Figure 3C). A BsMutL-Q487A variant conferred approximately a 50-fold mutator phenotype about 5-fold lower than a *mutL* null strain. Replacement of residues $^{487}QEMIV$ with five alanine residues also abrogated MMR *in vivo* (Figure 3C). This conserved loop is conspicuously exposed and loosely resembles the consensus β -binding motif (Dalrymple et al., 2001). Most notably, its conformation is nearly identical to that seen in the structures of other peptides bound to the β -clamp (Figure 3D). Superimposition of the $^{486}VQEMIVPL$ sequence from BsMutL onto the structures of β -clamp bound to peptides from polymerase II, FEN-1 and polymerase IV returned r.m.s. deviations smaller than 0.5 Å. Accordingly, the regulatory subdomains of both BsMutL and EcMutL could be directly docked onto the structure of the *E. coli* β -clamp. Interestingly, docking of the MutL-CTD dimer suggests that the interaction of one protomer

would prevent the interaction of the other due to steric hindrance (Figure S2), suggesting a possible regulatory role for this interaction.

A model for the activation of the endonuclease activity

Based on the structures of BsMutL-CTD, we suggest that the conserved motifs in MutL define an endonuclease active site with two distinct subsites. A structural Zn²⁺-binding site defined by the side chains of Glu468, Cys604 and His606; and a catalytic site likely defined by Asp462 and His464. Metal binding at the structural site locks the orientation between the dimerization and regulatory subdomains, which is highly variable in the absence of metal (Movie S1). Based on the three-dimensional organization of Asp462 and His464, the catalytic subsite could coordinate one or two metal ions to nick DNA (Yang, 2008). Supporting this idea, double-stranded DNA could be modeled onto the structure of BsMutL-CTD with the scissile bond at a distance compatible with catalysis activated by Asp462 and the adjacent 3' phosphate providing the fourth coordination ligand of the regulatory Zn²⁺ ion (Figure S3).

In the context of the replication fork, the endonuclease activity of MutL ought to be repressed until a mismatch is encountered. A look at the electrostatic potential surface of BsMutL-CTD reveals a powerful suppression mechanism of DNA-binding. The regulatory subdomain is covered with negative charges that guard the endonuclease site (Figure 4A). This could be a widely spread repression mechanism since some of the negatively charged residues in helix α C are conserved in other MutL homologues harboring the endonuclease motif (Figure 1C and (Kosinski et al., 2008)). Licensing the endonuclease activity of MutL would thus require a significant conformational change or the interaction with other repair factors to overcome the DNA repulsion in the vicinity of the endonuclease site. We presume that a conformational change like that induced in MutL α upon nucleotide binding could allow DNA bound at the ATPase domain to reach the endonuclease site (Sacho et al., 2008). However, additional repair factors are likely required to mask helix α C.

The endonuclease activity of MutL α is greatly stimulated by the presence of PCNA and RFC (Kadyrov et al., 2006; Kadyrov et al., 2007), the eukaryotic homologues of the β -clamp and the clamp loader. Additionally, MutS α and PCNA form a stable complex (Iyer et al., 2008). Human MutL α interacts with MutS α through its ATPase domain (Plotz et al., 2006), but the region of MutS α that interacts with MutL α is not known. Conceivably, the three proteins could form a ternary complex involved in strand discrimination, however, whether MutS α and MutL α can interact simultaneously with PCNA is controversial (Dzantiev et al., 2004; Lee and Alani, 2006). Bacterial MutS has two binding sites for the β -clamp (Lopez de Saro et al., 2006; Simmons et al., 2008). In *B. subtilis*, the C-terminal site is necessary to recruit MutL to mismatches and to activate the MMR response (Simmons et al., 2008). We presume that the ATPase domain of MutL could interact with MutS, while its C-terminal domain interacts with the β -clamp (Figure 4B). This model is supported by the presence of the β -binding like motif (⁴⁸⁷QEMIV) within the C-terminal domain of MutL and the fact that a PCNA binding sequence has been identified in the dimerization region of yeast MLH1 (Lee and Alani, 2006).

Collectively, our data pose an attractive model where the endonuclease activity of MutL is repressed by impaired DNA binding. Based on this data the simplest mechanism would harness MutL and β -clamp allowing for DNA binding and licensing of the endonuclease activity. Consequently, the structure provides a platform for future mechanistic studies of MutL-MutS- β at the early steps of mismatch repair.

Experimental Procedures

See the Supplemental Information for a more complete description of the methods. His-tagged BsMutL was purified using a Ni²⁺-chelating affinity, ionic exchange and size exclusion chromatography and stored in 20 mM TRIS pH 8, 100 mM KCl, 1 mM DTT and 5% glycerol (storage buffer). Purification of BsMutL-CTD (residues 433-627) included an additional ionic exchange purification step after His-tag cleavage with TEV-protease. Crystals were grown by vapor diffusion and optimized using streak seeding. Crystal form I was determined by MAD using a Sel-Met labeled crystal, while crystal forms II and III were solved by molecular replacement. Zinc-affinity assays were measured by incubating each BsMutL-CTD variant with increasing concentrations of ZnCl₂ in the presence of the fluorescent indicator FluoZin-3 (Fluka). Endonuclease and mismatch repair assays were performed largely as described (Kadyrov et al., 2006; Simmons et al., 2008).

Supplementary Material

Refer to Web version on PubMed Central for supplementary material.

Acknowledgments

We thank Michael d'Elia, Pablo Romero and the PXRR staff at NSLS-BNL for technical assistance. We are grateful to Drs. Junop and Ortega for critical reading of the manuscript. This work was supported by the National Sciences and Engineering Research Council of Canada (288295 to A.G.), the German Science Foundation (FR-1495/4-1 to P.F.), start-up funds from the University of Michigan (to L.A.S.) and the National Institutes of Health (CA21615 to G.C.W. and GM45190 to P.M.). M.C.P. is supported by an NSERC scholarship and G.C.W. is an American Cancer Society Research Professor.

References

- Ban C, Junop M, Yang W. Transformation of MutL by ATP binding and hydrolysis: a switch in DNA mismatch repair. *Cell*. 1999; 97:85–97. [PubMed: 10199405]
- Dalrymple BP, Kongsuwan K, Wijffels G, Dixon NE, Jennings PA. A universal protein-protein interaction motif in the eubacterial DNA replication and repair systems. *Proc Natl Acad Sci U S A*. 2001; 98:11627–11632. [PubMed: 11573000]
- Duppatla V, Bodda C, Urbanke C, Friedhoff P, Rao DN. The carboxy-terminal domain is sufficient for endonuclease activity of *Neisseria gonorrhoeae* MutL. *Biochem J*. 2009
- Dzantiev L, Constantin N, Genschel J, Iyer RR, Burgers PM, Modrich P. A defined human system that supports bidirectional mismatch-provoked excision. *Mol Cell*. 2004; 15:31–41. [PubMed: 15225546]
- Erdeniz N, Nguyen M, Deschenes SM, Liskay RM. Mutations affecting a putative MutLalpha endonuclease motif impact multiple mismatch repair functions. *DNA Repair (Amst)*. 2007; 6:1463–1470. [PubMed: 17567544]
- Guarné A, Junop MS, Yang W. Structure and function of the N-terminal 40 kDa fragment of human PMS2: a monomeric GHL ATPase. *Embo J*. 2001; 20:5521–5531. [PubMed: 11574484]
- Guarné A, Ramon-Maiques S, Wolff EM, Ghirlando R, Hu X, Miller JH, Yang W. Structure of the MutL C-terminal domain: a model of intact MutL and its roles in mismatch repair. *EMBO J*. 2004; 23:4134–4145. [PubMed: 15470502]
- Hall MC, Shcherbakova PV, Kunkel TA. Differential ATP binding and intrinsic ATP hydrolysis by amino-terminal domains of the yeast Mlh1 and Pms1 proteins. *J Biol Chem*. 2002; 277:3673–3679. [PubMed: 11717305]
- Iyer RR, Pohlhaus TJ, Chen S, Hura GL, Dzantiev L, Beese LS, Modrich P. The MutSalphaproliferating cell nuclear antigen interaction in human DNA mismatch repair. *J Biol Chem*. 2008; 283:13310–13319. [PubMed: 18326858]
- Kadyrov FA, Dzantiev L, Constantin N, Modrich P. Endonucleolytic function of MutLalpha in human mismatch repair. *Cell*. 2006; 126:297–308. [PubMed: 16873062]

- Kadyrov FA, Holmes SF, Arana ME, Lukianova OA, O'Donnell M, Kunkel TA, Modrich P. *Saccharomyces cerevisiae* MutLa is a mismatch repair endonuclease. *J Biol Chem.* 2007
- Kosinski J, Plotz G, Guarné A, Bujnicki JM, Friedhoff P. The PMS2 subunit of human MutLalpha contains a metal ion binding domain of the iron-dependent repressor protein family. *J Mol Biol.* 2008; 382:610–627. [PubMed: 18619468]
- Kosinski J, Steindorf I, Bujnicki JM, Giron-Monzon L, Friedhoff P. Analysis of the quaternary structure of the MutL C-terminal domain. *J Mol Biol.* 2005; 351:895–909. [PubMed: 16024043]
- Kunkel TA, Erie DA. DNA mismatch repair. *Annu Rev Biochem.* 2005; 74:681–710. [PubMed: 15952900]
- Lee SD, Alani E. Analysis of interactions between mismatch repair initiation factors and the replication processivity factor PCNA. *J Mol Biol.* 2006; 355:175–184. [PubMed: 16303135]
- Li GM, Modrich P. Restoration of mismatch repair to nuclear extracts of H6 colorectal tumor cells by a heterodimer of human MutL homologs. *Proc Natl Acad Sci U S A.* 1995; 92:1950–1954. [PubMed: 7892206]
- Lipkin SM, Wang V, Jacoby R, Banerjee-Basu S, Baxevanis AD, Lynch HT, Elliott RM, Collins FS. MLH3: a DNA mismatch repair gene associated with mammalian microsatellite instability. *Nat Genet.* 2000; 24:27–35. [PubMed: 10615123]
- Lopez de Saro FJ, Marinus MG, Modrich P, O'Donnell M. The beta sliding clamp binds to multiple sites within MutL and MutS. *J Biol Chem.* 2006; 281:14340–14349. [PubMed: 16546997]
- Mauris J, Evans TC. Adenosine triphosphate stimulates Aquifex aeolicus MutL endonuclease activity. *PLoS One.* 2009; 4:e7175. [PubMed: 19777055]
- Modrich P. Mechanisms in eukaryotic mismatch repair. *J Biol Chem.* 2006; 281:30305–30309. [PubMed: 16905530]
- Peltomaki P. Lynch syndrome genes. *Fam Cancer.* 2005; 4:227–232. [PubMed: 16136382]
- Plotz G, Welsch C, Giron-Monzon L, Friedhoff P, Albrecht M, Piiper A, Biondi RM, Lengauer T, Zeuzem S, Raedle J. Mutations in the MutSalphalpa interaction interface of MLH1 can abolish DNA mismatch repair. *Nucleic Acids Res.* 2006; 34:6574–6586. [PubMed: 17135187]
- Raschle M, Marra G, Nystrom-Lahti M, Schar P, Jiricny J. Identification of hMutLbeta, a heterodimer of hMLH1 and hPMS1. *J Biol Chem.* 1999; 274:32368–32375. [PubMed: 10542278]
- Sacho EJ, Kadyrov FA, Modrich P, Kunkel TA, Erie DA. Direct visualization of asymmetric adenine-nucleotide-induced conformational changes in MutL alpha. *Mol Cell.* 2008; 29:112–121. [PubMed: 18206974]
- Simmons LA, Davies BW, Grossman AD, Walker GC. Beta clamp directs localization of mismatch repair in *Bacillus subtilis*. *Mol Cell.* 2008; 29:291–301. [PubMed: 18280235]
- Yang W. An equivalent metal ion in one- and two-metal-ion catalysis. *Nat Struct Mol Biol.* 2008; 15:1228–1231. [PubMed: 18953336]
- Zhang Y, Yuan F, Presnell SR, Tian K, Gao Y, Tomkinson AE, Gu L, Li GM. Reconstitution of 5'-directed human mismatch repair in a purified system. *Cell.* 2005; 122:693–705. [PubMed: 16143102]

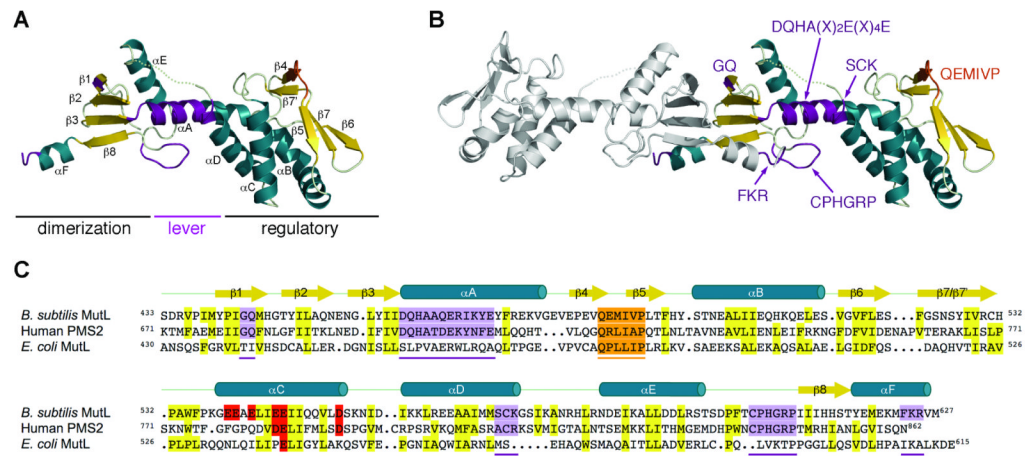


Figure 1. Crystal structure of BsMutL-CTD

(A) Ribbon diagram of the BsMutL-CTD monomer. Secondary structure motifs are labeled and colored blue (helices) and yellow (strands) with the connecting loops in light green. The endonuclease and the endonuclease-associated motifs are shown in purple, while the additional conserved motifs are shown in orange. (B) Ribbon diagram of the BsMutL-CTD dimer with one protomer shown as in (a) and the other one as grey ribbons. (C) Sequence alignment of the C-terminal regions of BsMutL, hPMS2 and EcMutL. Secondary structure elements of BsMutL-CTD are shown as arrows (strands) and cylinders (helices). The five conserved motifs are highlighted in purple and underlined. Conserved hydrophobic residues are highlighted in yellow. The conserved ⁴⁸⁷QEMIVP motif is highlighted in orange. See also Figure S1.

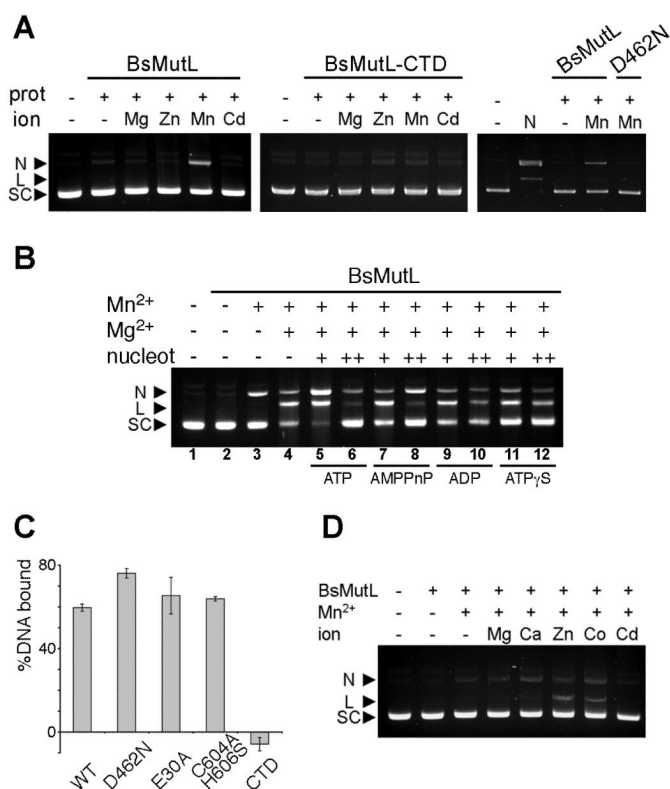


Figure 2. Endonuclease activity of BsMutL

(A) Nicking activity of BsMutL (left) and BsMutL-CTD (center) in the presence of Mg²⁺, Zn²⁺, Mn²⁺ or Cd²⁺ as indicated. Comparison of the nicking activity of BsMutL and BsMutL-D462N in the presence of Mn²⁺ (right). Migration of supercoiled (SC), nicked (N) and linear (L) DNA is indicated. (B) Endonuclease activity of BsMutL in the presence of 0.5 mM (+) and 5 mM (++) nucleotide. (C) DNA binding by BsMutL (WT), BsMutL-CTD (CTD) and BsMutL variants as indicated. Data are presented as the mean of three independent measurements and the error bars correspond to the standard errors of the mean (SEM= σ/\sqrt{n} , where σ is the average and n the sample size). (D) Stimulation of the endonuclease activity of BsMutL (1 mM Mn²⁺) by a second divalent metal ion (1 mM).

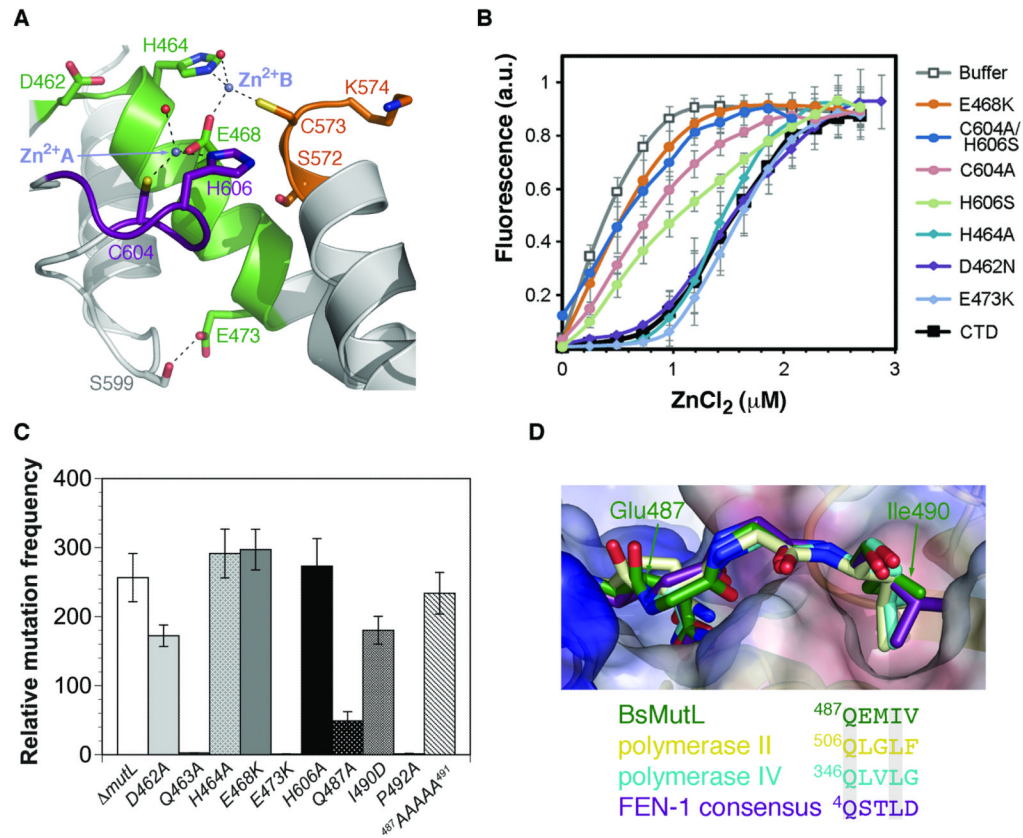


Figure 3. Regulatory Zn²⁺-binding site in BsMutL-CTD

(A) Organization of the endonuclease site of BsMutL-CTD bound to Zn²⁺ (crystal form III). Hydrogen bonds are shown as black dashed lines with the water molecules and Zn²⁺ ions shown as red and lilac spheres, respectively. Conserved motifs are color-coded green (⁴⁶²DQHAX₂EX₄E), purple (⁶⁰⁴CPHGRP) and orange (⁵⁷²SCK). (B) Zinc-affinity profiles of BsMutL-CTD and point mutants of BsMutL-CTD as indicated. (C) Bar diagram showing the relative mutation frequency of the indicated *mutL* variants altered in the Zn²⁺-binding, the endonuclease site and the putative β-binding motif. Data are presented as the mean of 4 independent cultures +/- SEM. (D) Superimposition of the β-binding motif in BsMutL-CTD (green) onto those of pol II (yellow, PDB 3D1E), pol IV (cyan, PDB 1UNN) and FEN-1 (purple, PDB 1RXM) shown as a main-chain trace with the β-clamp structure (PDB 3D1E) presented as a semi-transparent electrostatic potential surface. See also Figures S2-S3 and Movie S1.

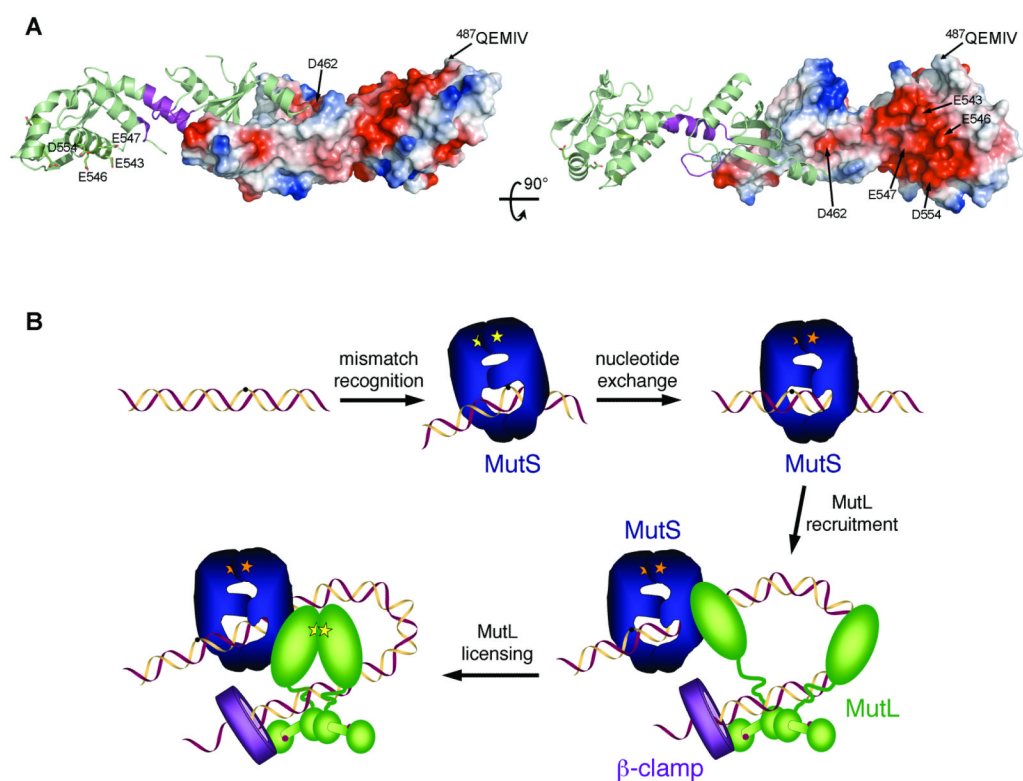


Figure 4. Model of activation of the endonuclease activity of MutL

(A) Orthogonal views of the electrostatic surface potential of the BsMutL-CTD protomer. The second protomer is shown as a ribbon diagram with the endonuclease motifs in purple. (B) Upon mismatch binding, MutS (blue) undergoes a nucleotide-dependent conformational change that triggers recruitment of MutL (green) to the mismatch site, likely aided by the β -clamp (purple). ATP binding by MutL then promotes the association of its two ATPase subunits and brings the ATPase in close proximity to the dimerization domain of the protein. Coordinated interaction of MutS and β -clamp bound to DNA (ribbon diagram) with ATP-bound MutL could thus license the latent endonuclease activity of MutL. ATP and ADP are shown as yellow and orange stars, respectively.

Table 1

Data Collection and Refinement

Data Collection	Crystal Form I			Crystal Form II		Crystal Form III		
	C222 ₁			P2 ₁ 2 ₁ 2 ₁		P2 ₁ 2 ₁ 2 ₁		
Unit Cell (Å)	a=88.3, b=94.9, c=218.7							a=33.2, b=74.6, c=182.2
Wavelength (Å)	0.9794 (Se-edge)	0.9792 (Se-peak)	0.9686 (Se-remote)	1.0809 (native)	1.282 (Zn-peak)	1.2796 (Zn-peak)		
Resolution (Å) ^a	35-2.8 (2.9-2.8)	35-2.8 (2.9-2.8)	35-2.8 (2.9-2.8)	50-2.38 (2.47-2.38)	50-2.0 (2.03-2.00)	50-2.15 (2.19-2.15)		
Completeness (%) ^a	98.2 (88.3)	98.6 (91.4)	92.5 (55.9)	95.9 (76.0)	100 (100)	99.3 (93.3)		
Redundancy ^a	6.2 (5.0)	6.3 (5.4)	6.3 (3.9)	5.5 (4.5)	7.5 (7.4)	10.3 (6.3)		
Rmerge (%) ^a	6.5 (21.0)	8.1 (21.3)	7.2 (23.1)	4.0 (22.5)	8.3 (67.6)	8.9 (70.7)		
I/σ(I) ^a	20.2 (6.9)	18.5 (5.6)	17.8 (4.9)	41.5 (4.5)	25.9 (3.1)	22.4 (2.3)		
ASU content	4 monomers			4 monomers	1 dimer	1 dimer		
Data Refinement								
Resolution (Å)				30-2.5	38.9-2.0	32.8-2.3		
Reflections (work)				31,772	60,020	41,004		
Reflections (test)				1,631	3,049	2,113		
Atoms refined				6,122	3,294	3,120		
Solvent atoms				105	190	74		
Zn atoms				--	--	4		
R (R _{free}) (%)				21.7 (26.8)	19.1 (22.8)	21.4 (26.9)		
Rmsd in bonds (Å)				0.003	0.005	0.004		
Rmsd in angles (°)				0.609	0.875	0.745		
Mean B values (Å)				44.1	45.6	43.9		

^aData in the highest resolution shell is shown in parentheses.